Turkish Journal of Electrical Engineering & Computer Sciences

http://journals.tubitak.gov.tr/elektrik/

Research Article

Turk J Elec Eng & Comp Sci
(2017) 25: 1197 – 1210

doi:10.3906/elk-1507-259

Implementation of a flywheel energy storage system for space applications

Reşat ÇELİKEL[1,*], **Mehmet ÖZDEMİR**[2], **Ömür AYDOĞMUŞ**[3]

[1]Electrical Program, Çüngüş Mehmet Adıgüzel Vocational High School, Dicle University, Diyarbakır, Turkey
[2]Department of Electrical and Electronics Engineering, Fırat University, Elazığ, Turkey
[3]Department of Mechatronics Engineering, Technology Faculty, Fırat University, Elazığ, Turkey

Received: 30.07.2015 • **Accepted/Published Online:** 09.04.2016 • **Final Version:** 10.04.2017

Abstract: A satellite power system requires solar panels to provide energy and orientation. There are two regions in the orbital path of the satellite: the dark and bright region. The energy is provided by solar panels in the bright region and by flywheel energy storage system (FESS) in the dark region. Brushless DC (BLDC) motors are widely used in the FESS due to their low weight, high power density, high efficiency, high reliability, and high speed. Some mechanical resonances may occur due to physical features of the mechanical parts. Therefore, the current of the BLDC is dramatically increased because of the mechanical resonance. In this work, a current reference method was used to protect the power systems of the satellite from the current spikes of the solar power system. The parameters of the PI controller were calculated by using genetic algorithms. A FESS was designed and experimentally performed for high speed operation at about 20 krpm in the vacuumed environment.

Key words: Brushless motors, current reference method, energy storage, flywheel, genetic algorithms

1. Introduction

There have been many works related to energy extraction from flywheels in the last two decades. The flywheel energy storage system (FESS) has been used for power smoothing in the grid, transport/hybrid vehicles, and UPS applications [1–10]. In particular, satellite power systems use the FESS, as presented in [11,12].

Satellites stay in the bright region for about an hour and in the dark region for about half an hour during their routine orbit. The required energy is provided by a mechanical energy storage unit or electro-chemical batteries when operating in the dark region. In the bright region, the mechanical energy is stored in the FESS, and then the stored energy is used in the dark region.

The FESS consists of a high speed brushless DC (BLDC) motor, a variable frequency motor drive, a flywheel, a coupling between motor and flywheel, a high speed bearing with low friction, and a vacuum chamber.

BLDC motors are widely used in industrial applications such as automotive technology, appliances, medical, industrial automation equipment, and aerospace application. In aero applications, BLDC motors are used owing to their low weight, high power density, high efficiency, and high reliability [13–15]. High speed BLDC motors are usually used in the FESS. The high speed BLDC motor is used in the FESS with charge mode (bright region) and discharge mode (dark region).

The motor current is increased and reaches maximum motor current when the mechanical resonance

*Correspondence: resat.celikel@gmail.com

occurs in the conventional speed control system. The current control of the BLDC motor is an important problem in the charge mode because undesirable current spikes occur in mechanical resonances. The undesirable current spikes cause the high price of solar panels [16]. Therefore, the current reference method (CRM) is used to reduce the cost of solar panels and the volume of the system. In addition, the power system of the satellite is protected from current spikes by using the CRM. Thus, the changing load of the BLDC motor does not affect the current of the power system. If the power demand rises owing to an increase in BLDC motor current, the solar panel will increase in size and cost. Therefore, the CRM has been used to eliminate the effect of disturbances. The current reference is generated in order to reach the determined speed of the flywheel in the CRM.

Calculation of system losses is used to produce current reference. The speed of the motor is changed when the disruptive impact occurs. However, the motor current does not change in this case. The value of reference current is determined according to the desired system speed value.

The current controller is obtained by using a traditional PI controller structure because of its simple structure, easy design, and low cost [17]. In this work, the parameters of the PI controller have been determined by genetic algorithm (GA). The high speed BLDC motor has a low winding inductance due to its winging layout and structure. Therefore, a filter must be used between motor and inverter to reduce the current ripples and total harmonic distortion (THD). PI parameters can be determined by using an extended transfer function that consists of a PI controller, filters, BLDC, inverter, and current sensor. The values of Proportional (P) and Integral (I) are calculated by GA, a type of stochastic algorithm based on the principles of natural selection and genetics. These robust GAs have been successfully applied to problems in a variety of fields of study, and their popularity continues to increase due to their effectiveness, their applicability, and their ease of use [18].

In this paper, a FESS has been designed with a high speed BLDC motor and a flywheel operated in a vacuumed environment. The system performances were experimentally presented via current spike and speed in the resonance region. The DC current and speed were measured from zero speed to maximum speed. The flywheel speed reached the desired speed at the determined time by using only the P controller. The harmonic spectrum of motor current was shown in the steady state speed. The current spikes were eliminated as expected in the resonance region by the proposed current.

2. Modeling of the FESS

A BLDC motor has three-phase stator windings and permanent magnets on the rotor. The rotor position is determined with Hall-effect sensors at each 60°. The position information of sensors is required for electronic commutation, which is performed by a voltage source inverter. The two different phase windings are energized at each 60° by using the information of the rotor position [19].

The block diagram of the current controlled FESS is shown in Figure 1. The FESS consists of solar panels, an inverter, LC filter, BLDC motor, flywheel, and sensors.

2.1. Modeling of the BLDC motor

The mathematical model of the BLDC motor is given in Eqs. (1) to (5). Current reference of the BLDC motor is defined by Eqs. (6) and (7).

$$\begin{bmatrix} V_a \\ V_b \\ V_c \end{bmatrix} = \begin{bmatrix} R & 0 & 0 \\ 0 & R & 0 \\ 0 & 0 & R \end{bmatrix} \begin{bmatrix} I_a \\ I_b \\ I_c \end{bmatrix} + \begin{bmatrix} L & 0 & 0 \\ 0 & L & 0 \\ 0 & 0 & L \end{bmatrix} \frac{d}{dt} \begin{bmatrix} I_a \\ I_b \\ I_c \end{bmatrix} + \begin{bmatrix} e_a \\ e_b \\ e_c \end{bmatrix}, \tag{1}$$

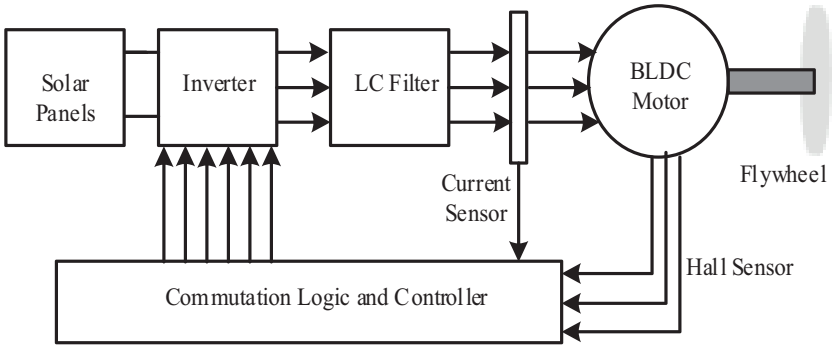

Figure 1. CRM and flywheel energy storage system.

where R is the phase resistance; L is the phase inductance; $e_a, e_b,$ and e_c are the phase back EMFs; and $I_a, I_b,$ and I_c are the phase currents of the BLDC motor.

The two-phase conduction mode is preferred in the BLDC motor drive because of simple switching.

$$V = i_s R_s + L_s \frac{di_s}{dt} + E_z \tag{2}$$

$$E_z = K_e \omega_m \tag{3}$$

$$T_m = T_L + J\frac{d\omega_m}{dt} + B\omega \tag{4}$$

$$T_m = K_t i_s \tag{5}$$

$$T_{mech}\omega_m = i_s E_z = P_{mech} \tag{6}$$

$$i_{ref} = \frac{P_{acc} + P_{fr} + P_{wnd}}{E_z}, \tag{7}$$

where V is the armature voltage, i_s is the armature current, R_s is the armature resistance, L_s is the armature inductance, E_z is the back EMF voltage, K_e is the back EMF constant, K_t is the torque constant, T_m is the torque developed by the motor, T_{mech} is the torque mechanic by developed the motor, ω_m is the angular speed, J is the moment inertia of motor and flywheel load, B is the frictional constant of motor and load, P_{mech} is the power mechanic of motor, P_{acc} is the power acceleration, P_{fr} is the power friction of motor and load, and P_{wind} is the power winding of load.

Eqs. (2) to (6) are determined from the two-phase conduction mode. The current reference is obtained by Eq. (7). The transfer function of the BLDC motor is obtained by Eqs. (8) and (9).

$$V(s) = i_s(s)R_s + sL_s i_s(s) + K_e\omega_m(s) \tag{8}$$

$$K_t i_s(s) = T_L + Js\omega_m(s) + B\omega_m(s) \tag{9}$$

The transfer function of the BLDC motor is shown in Eq. (10) for current control.

$$\frac{i_s(s)}{V(s)} = \frac{Js + B}{L_s Js^2 + (R_s J + L_s B)s + R_s B + K_e K_t} \tag{10}$$

2.2. Modeling of the inverter, current sensor, flywheel, and LC filter

The inverter and current sensor are defined by a simple transfer function involving occurred gain and time constant. The time constant is associated with switching frequency of the inverter. The gains are determined as conversion rate. The conversion rate depends on the structure of the inverter and current sensor. The transfer functions of the inverter and the current sensor are given by Eqs. (11) and (12), respectively.

$$T_c(s) = \frac{K_c}{T_c s + 1} \tag{11}$$

$$T_a(s) = \frac{K_a}{T_a s + 1}, \tag{12}$$

where T_c is the inverter time constant, K_c is the inverter gain, T_a is the current sensor time constant, and K_a is the current sensor gain. Power losses of the system must be calculated for the current reference produced. These losses occurred by friction of air and bearing. The calculation of air friction loss is given in Eqs. (13) to (16). The flywheel is placed into a housing vacuumed for reducing air friction. The shape of the flywheel is shown in Figure 2 [20].

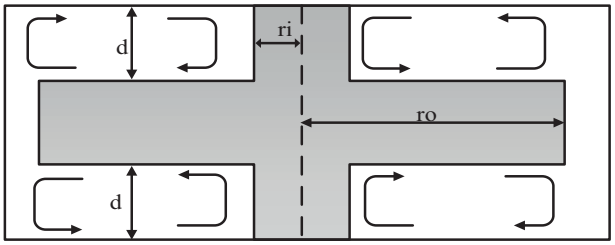

Figure 2. Shape of flywheel.

$$P_{wnd} = k_f \times M_{disc} \times \omega_m \tag{13}$$

$$C_f = \frac{3.7 \times \left(\frac{d}{r_o}\right)^{0.1}}{\sqrt{R_e}} \tag{14}$$

$$M_{disc} = \frac{\left[\left(C_f \times \rho_a \times \omega_m^3\right)\left(r_o^5 - r_i^5\right)\right]}{2} \tag{15}$$

$$R_e = \frac{\rho_a \times \omega_m^2 \times r_o^2}{\mu}, \tag{16}$$

where k_f is the smoothness coefficient, R_e is the Reynolds coefficient, ρ_a is the air density, and r_i and r_o are the inner and outer radius of flywheel, respectively. $\mu\mu$ is the dynamic viscosity of air.

In this application, a high speed hybrid bearing with low viscosity grease oil has been used for high speed operation. Calculation of the friction losses of the bearing are given in Eqs. (17) to (22).

$$P_{fr} = (M_0 + M_1)\omega_m \tag{17}$$

$$M_0 = f_0 \times (v \times n)^{\frac{2}{3}} \times d_m^3 \times 10^{-10} \tag{18}$$

$$M_1 = f_1 \times P_1 \times d_m \tag{19}$$

$$P_1 = \omega_m \left(F_r + F_b\right) \tag{20}$$

$$F_r = m \times g \tag{21}$$

$$F_b = m_r \times e \times \omega_m^2 \tag{22}$$

$$P_{acc} = J \times \omega_m \times \frac{\Delta\omega_m}{\Delta t} = J \times \omega_m \times \frac{\omega_2 - \omega_1}{t_2 - t_1}, \tag{23}$$

where f_0 and f_1 are coefficients of bearing, n is bearing speed, v is the kinematic viscous friction of bearing grease, m is the weight of flywheel, m_r is the residual mass, e is the eccentricity between the rotational axis of the flywheel and the mass center, and d_m is the average diameter of bearing. The current ripple is too high due to low motor inductance. High switching frequency is required because of the high fundamental frequency, 500 Hz/1 kHz. dv/dt stresses are seen on the motor winding because of high switching frequency. These voltage stresses must be reduced by using an LC filter [21]. The transfer function of the LC filter is given in Eq. (24) and the structure of the LC filter is shown in Figure 3.

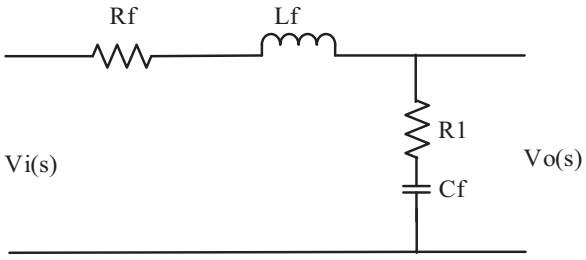

Figure 3. LC filter is one phase of the BLDC motor.

$$\frac{V_o}{V_i} = \frac{sC_fR_1 + 1}{s^2C_fL_f + s(C_fR_f + C_fR_1) + 1}, \tag{24}$$

where L_f is the filter inductance, R_f is the resistance of filter inductance, C_f is the filter capacitance, and R_1 is the damping resistance of the LC filter. It is typically recommended that the LC filter resonance frequency should be chosen three times lower that the power converter switching frequency. The corner frequency of the LC filter is selected as 15.93 kHz, which is shown in Eq. (25). The switching frequency of the inverter is taken as 53.6 kHz. The electrical frequency of the system is 332 Hz (20 krpm).

$$f_c = \frac{1}{2\pi\sqrt{L_fC_f}} \tag{25}$$

The block diagram of the entire system is illustrated in Figure 4. The system consists of a PI controller, a filter, an inverter, a BLDC motor, and a current sensor. Thus, the complex transfer function is obtained by using

the block diagram. The system parameters are given in [16,22–24]. PID is adjusted to minimize the magnitude of error, steady state error of system, and transient response of the system. The transfer function of the PID controller is shown in Eq. (26).

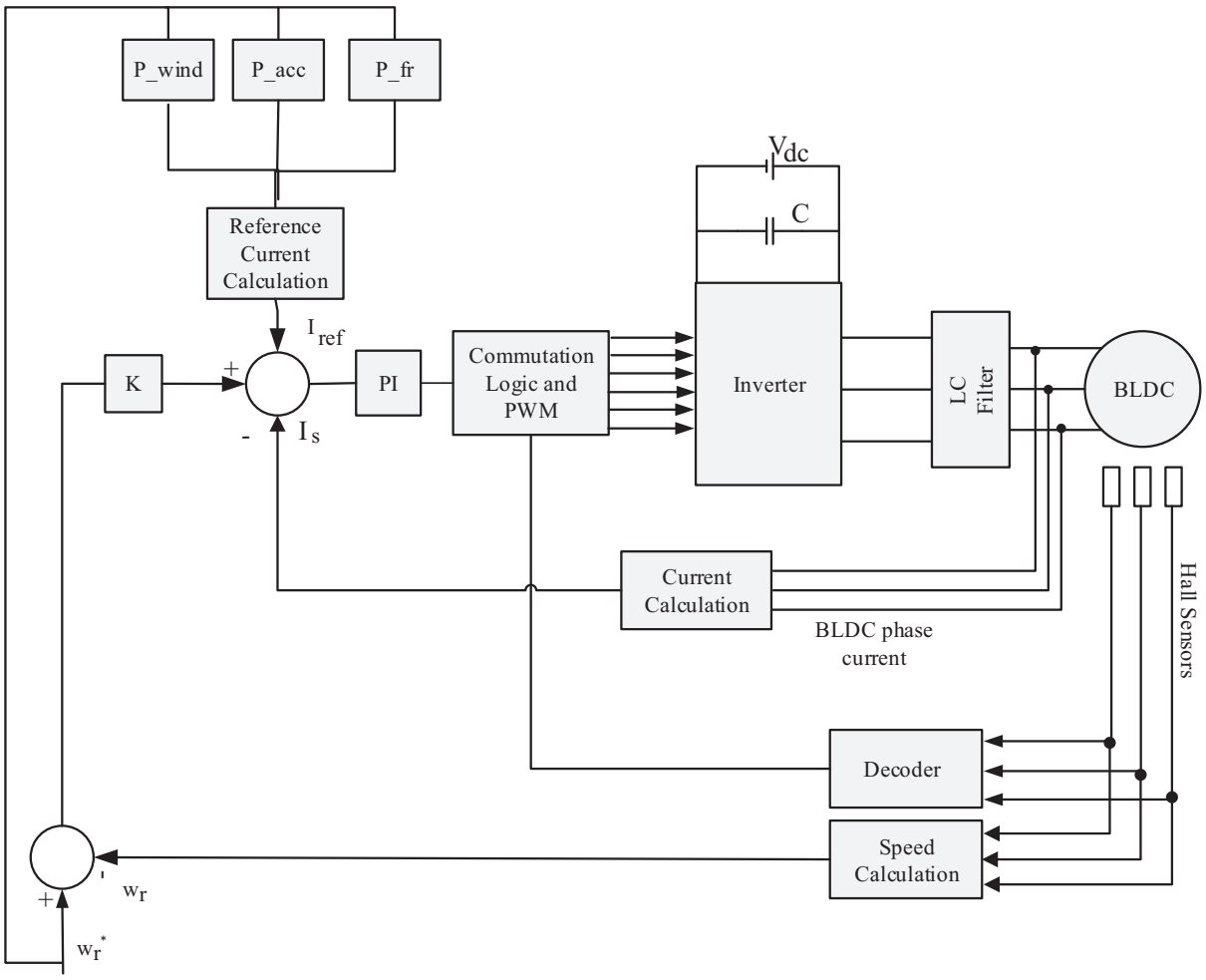

Figure 4. Block diagram of the FESS system.

$$PID(s) = \frac{s^2 k_d + s k_p + k_i}{s} \tag{26}$$

The closed-loop transfer function is controlled by a PI controller as shown in Figure 5. One of the methods of PID parameters tuning is the Ziegler–Nichols (Z-N) method. In the Z-N method of closed-loop, K_p is set and the system is brought to the point of oscillation [25]. While the system is at the oscillation point, ultimate gain K_u and ultimate period T_u are obtained. GA is an effective and efficient optimization technique using solutions of complicated problems based on evaluation of natural selection. GAs include three major operators: selection, crossover, and mutation, in addition to control parameters: population size, selection pressure, crossover, and mutation rate.

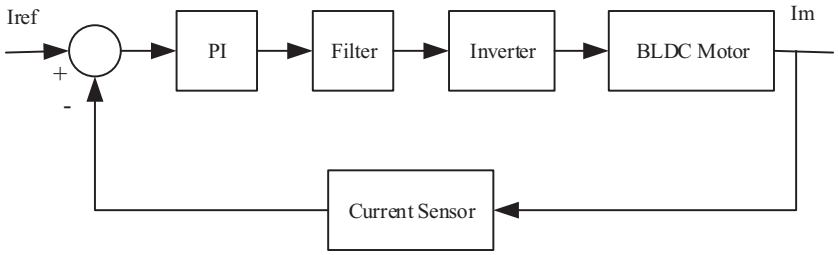

Figure 5. Block diagram of the FESS system for current control.

The pattern search method is a kind of direct search algorithm. Direct search methods are an important class of optimization algorithms that attempt to minimize a function by comparing its value in a finite set of trial points (computed by simple mechanisms). The pattern search (PS) optimization routine is an evolutionary technique that is suitable to solve a variety of optimization problems that lie outside the scope of the standard optimization methods. A historic discussion of direct search methods for unconstrained optimization is presented in reference [26]. The hybrid function is an important optimization function that solves complex problems to minimize the value of the fitness function. In this work, PID parameters have been obtained by GA/PS hybrid function.

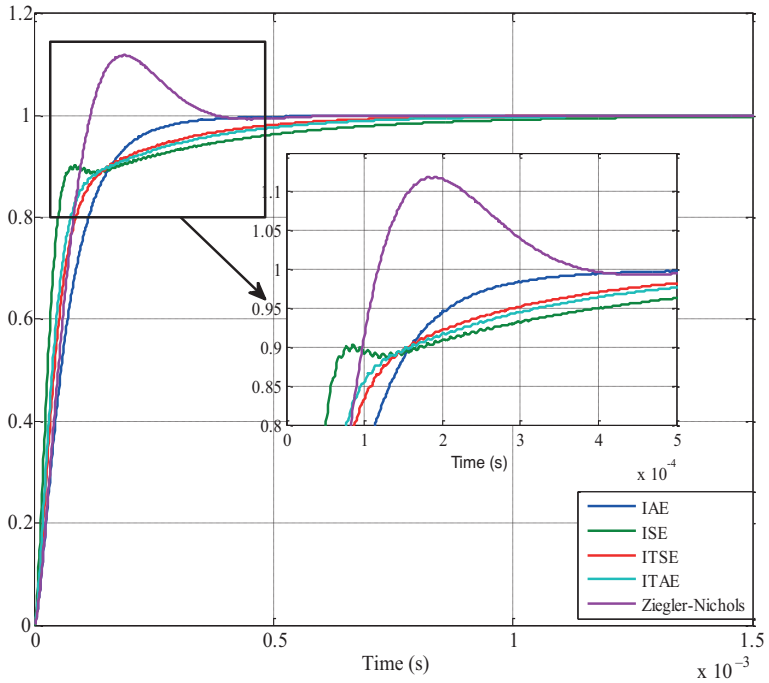

Figure 6. The unit step response of system with error criterion by using GA/PS and Ziegler–Nichols method.

Some error criteria are used in optimal calculation of the PID. These error criteria are integral of absolute error (IAE), mean squared error (MSE), integral of squared error (ISE), integral of time multiplied by absolute error (ITAE), and integral of time multiplied by squared error (ITSE). They have been applied in the system as unit step response of the system as shown in Figure 6. The integral absolute error criterion has obtained the optimal result according to the other error criteria. According to this result, the system performance values and k_p, k_i, k_d are given in the Table. The controller type has been selected as PID controller to determine the

parameters. However, the parameter of the derivative k_d is calculated from the GA optimization as zero. In addition, the Z-N method calculated the derivative k_d as almost zero. The parameters of the PI controller are calculated by using GA (GA parameters: K = 0.001, k_p = 0.088, k_i = 748.297, k_d = 0, and Z-N parameters: k_p = 0.08355, k_i = 1422.23, k_d = 3.27 × 10^{-6})

Table. The system performance values.

	Rise time (s)	Peak time (s)	Settling time (s)	Overshoot (%)
GA/PS-IAE	1.6×10^{-4}	9.3×10^{-4}	9.3×10^{-4}	0
Z-N	9.8×10^{-5}	1.8×10^{-4}	9.1×10^{-4}	11.9
	Kp	Ki	Kd	
GA/PS-IAE	0.088	748.297	0	
Z-N	0.08355	1422.23	3.27×10^{-6}	

3. Experimental results

The steady-state of speed value must reach the reference speed in about an hour in the bright region for satellite application. In this time zone, current spikes occur in the mechanical resonances and some of the distortions in the conventional direct speed control system. The elimination of the current spikes is the first aim of this work and is important for space applications.

The reaching of desired flywheel speed is the second aim of this work. The flywheel must reach the desired speed by using current reference. If the reference speed cannot be achieved, it may not have generated enough energy in the dark region. Current reference of the motor is generated by the continually increasing speed reference and back EMF. The direct speed controller was not used in the system. The reference power of motor acceleration is made zero when flywheel speed reaches the determined speed. The power of the BLDC motor exclusively provides losses at the maximum speed. The algorithm of the current reference is shown in Figure 7. In this algorithm, P_{acc} is determined depending on motor reference speed as shown in Eq. (27) and motor speed is measured to generate current error depending on the magnitude of the mechanical resonance. The amplitude of current error is calculated by Eq. (28). BLDC motor current is obtained by using motor phase current and it is given in Eq. (29). The experimental setup of the FESS is illustrated in Figure 8 with details of the flywheel. (1) The high speed BLDC "Maxon EC25", (2) Motor drive "ESCON 70/10", (3) Coupling between motor and flywheel "R+W MKS45", (4) High speed bearing "Aerospace Hybrid FAG bearing", (5) flywheel "T 601-Steel", (6) vacuum chamber "≈0bar", (7) vacuumed flywheel chase, (8) vacuum pump, (9) pressure measurement, (10) external microcontroller, (11) current clamp, (12) digital scope, (13) power supply, and (14) PC.

The phase current of the BLDC motor was measured by ESCON 70/10 driver. The sensitivity of the measurement depends on the analogue input of the external microcontroller mentioned in the paper. The current information is sent from the motor drive by using analogue output with 12-bit resolution (0–4 V). The motor current is approximately equal to the DC supply current and this supply current is shown in Figure 9. The motor parameters used have been obtained from the Maxon datasheet.

$$P_{acc} = \begin{pmatrix} n_{ref} = n_m, & P_{acc} = 0 \\ n_{ref} > n_m, & P_{acc} = -P_{acc} \\ n_{ref} < n_m, & P_{acc} = P_{acc} \end{pmatrix} \tag{27}$$

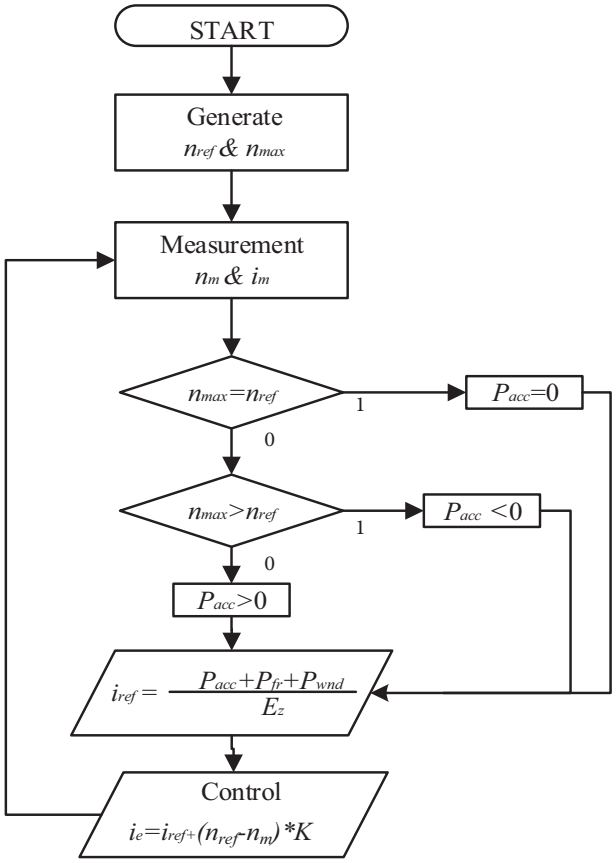

Figure 7. Algorithm to current reference produces.

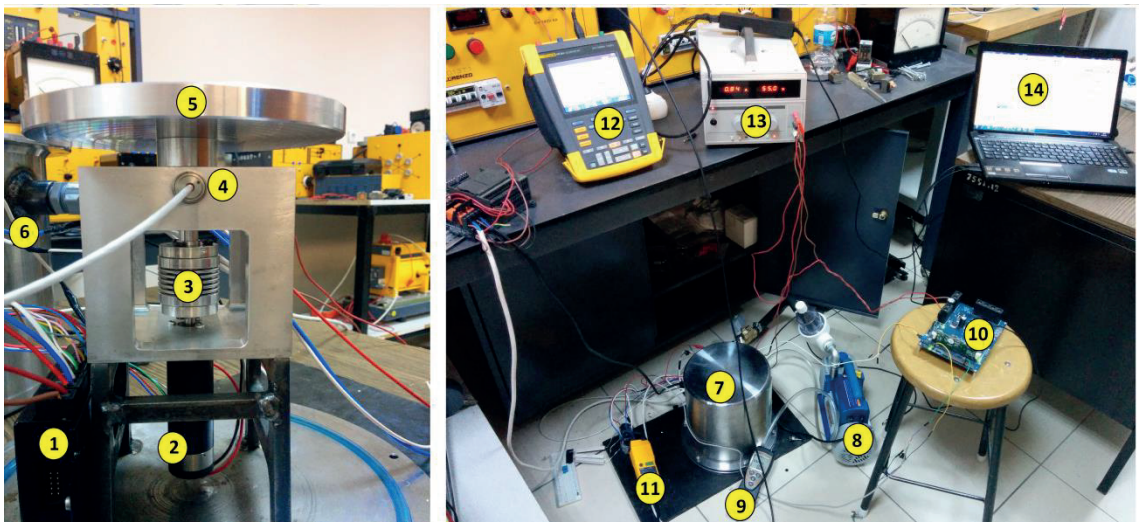

Figure 8. Photograph of the FESS with experimental setup.

$$e(t) = [(\omega_{ref} - \omega_m) \times K] + i_{ref} - i_s \tag{28}$$

$$I_s = \frac{I_a + I_b + I_c}{2} \tag{29}$$

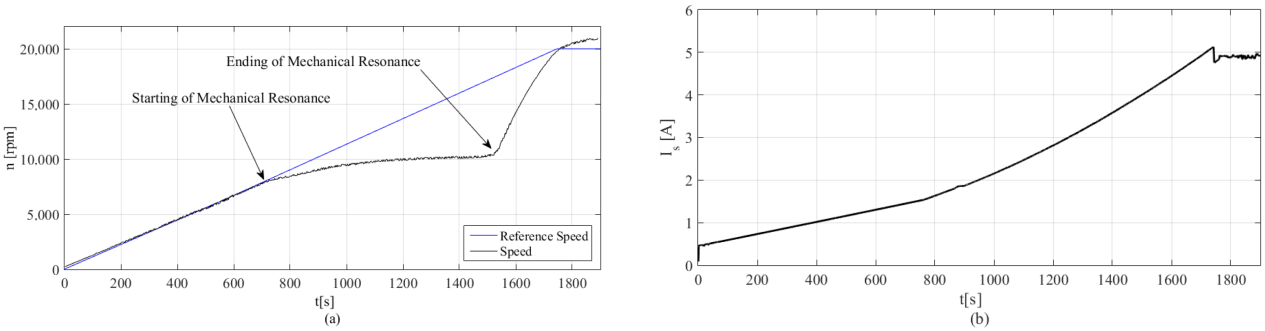

Figure 9. Conventional current control method: a) Reference and system speed, b) BLDC motor current.

Current reference is obtained by Eq. (7) and P_{wnd}, P_{fr}, and P_{acc} are shown Eqs. (13), (17), and (23), respectively. The parameters of the equations are obtained by bearing data and environment value. Only the value of $(m_r \times e)$ has been found experimentally. It was taken as 710 in Figure 9. Motor speed and commutation time were measured by using Hall-effect sensors.

The current reference has two parts: losses and acceleration. The first part is calculated by the system losses, which have bearing losses and winding losses. The second part is calculated by multiplication of the inertia torque and acceleration of speed. The current reference is generated via an external microcontroller (TMS320F28069) connected to a Maxon motor drive device.

The first experimental work was implemented to show the mechanical resonance problem as given in Figure 9. In the first work, a conventional current controller was used to control the system speed. The reference speed and flywheel speed are illustrated in Figure 9a. The mechanical resonance has been started in 700 s and finished in 1500 s. The mechanical resonance has not been overcome by the conventional current control method and the speed control has not been achieved by using this method as shown in Figure 9a. Moreover, the motor current has increased depending on the reference speed in the mechanical resonance region as given in Figure 9b.

This traditional control method is not suitable for mechanical systems that have mechanical resonances in the operating regions. The proposed control method is a good solution to overcome mechanical resonances and to perform the speed control of the system. Therefore, an effective current reference control method has been used for the FESS.

The same conditions and same speed reference were used to show the performance of the proposed controller as given in Figure 10. The motor current is approximately equal to the DC supply current and this supply current is shown in Figure 10. The value of $(m_r \times e)$ was taken as 665 in Figure 10. The mechanical resonance occurred approximately at the same point and the resonance has been overcome in a short time for the CRM. The flywheel speed has been controlled by the overlapped reference speed as shown in Figure 10a. The indirect speed control (only proportional gain) has been achieved by using the proposed controller for 20,000 rpm reference speed.

The motor current has been increased proportionally throughout the mechanical resonance period as given in Figure 10b. The increasing of the current value does not damage the satellite power system due to the fact that the current waveform has no current spike effect. Thus, di/dt current stresses do not occur on the switches.

The other experimental result was given to show harmonic contents of the motor current at the steady-state operation region, which is illustrated in Figure 11, to compare GA/PS and Z-N. The motor current was

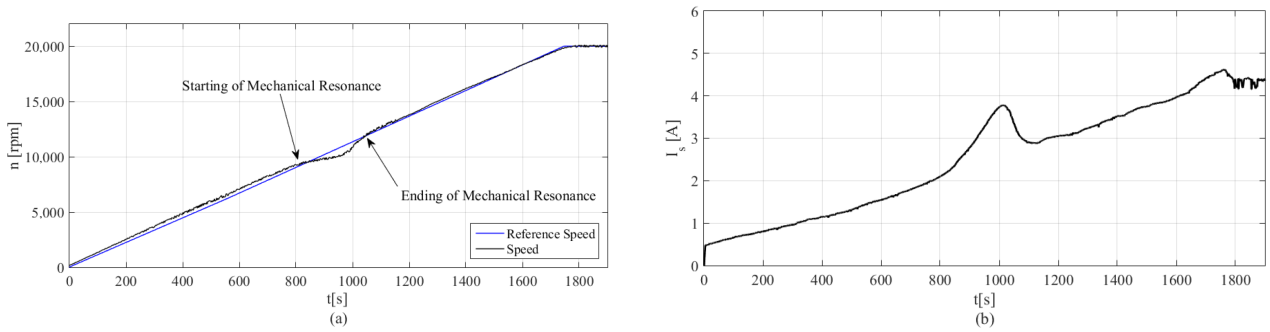

Figure 10. Proposed current control method: a) Reference and system speed, b) BLDC motor current.

measured at the 20,000 rpm speeds, which are shown in Figures 11a and 11b for GA/PS and Z-N controllers, respectively. The current THD are calculated about 25% for GA/PS and about 28% for Z-N, which are given in Figures 11c and 11d, respectively. The 5th harmonic order is about 19% of fundamental harmonic as given in detail in Figure 11c for GA/PS. However, the 5th harmonic order is about 21% of fundamental harmonic as shown in Figure 11d for Z-N.

4. Conclusions

A FESS was designed and used for some different experiments in this paper. The FESS was implemented using a high speed BLDC and a flywheel operated at 20 krpm in the vacuumed environment.

The PI parameters are determined by GA to obtain optimum performance for current control. Therefore, a transfer function is determined that consists of a PI controller, filters, BLDC, inverter, and current sensor.

Some mechanical resonances have occurred due to physical features of the mechanical parts of the FESS. Therefore, the speed of the flywheel cannot reach the reference speed because of the mechanical resonance by the traditional control method. Therefore, an effective current reference method has been proposed to overcome

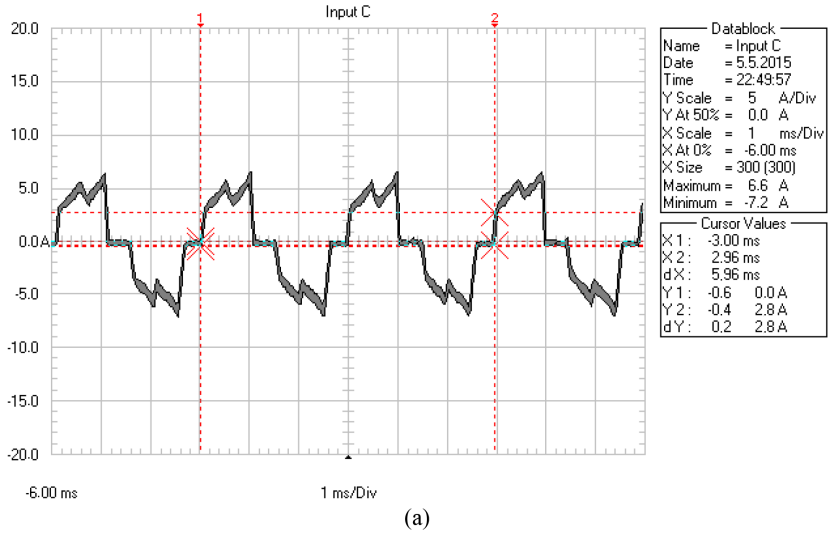

Figure 11. Steady-state at 20,000 rpm: a) A phase current of motor for GA/PS, b) A phase current of motor for Z-N, c) Harmonic spectrum of motor current for GA/PS, c) Harmonic spectrum of motor current for Z-N.

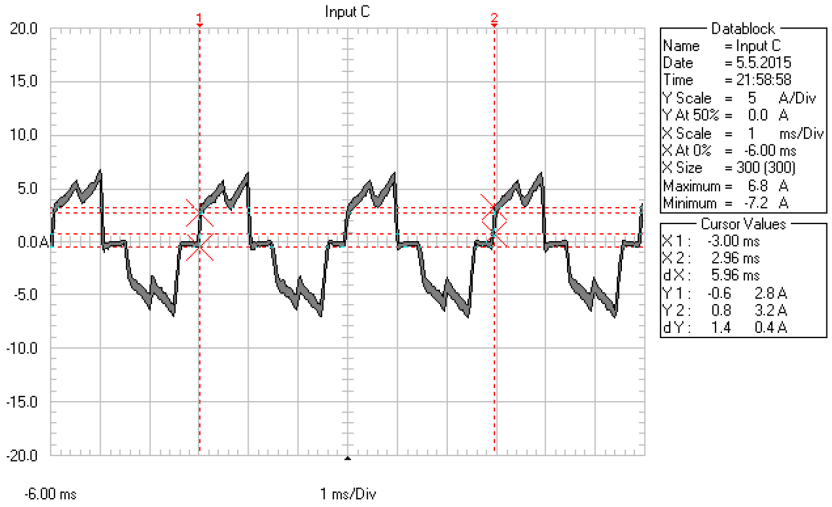

(b)

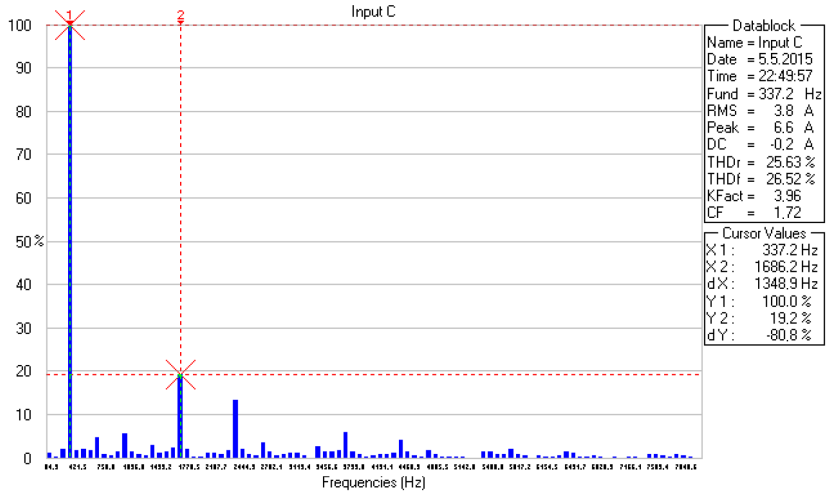

(c)

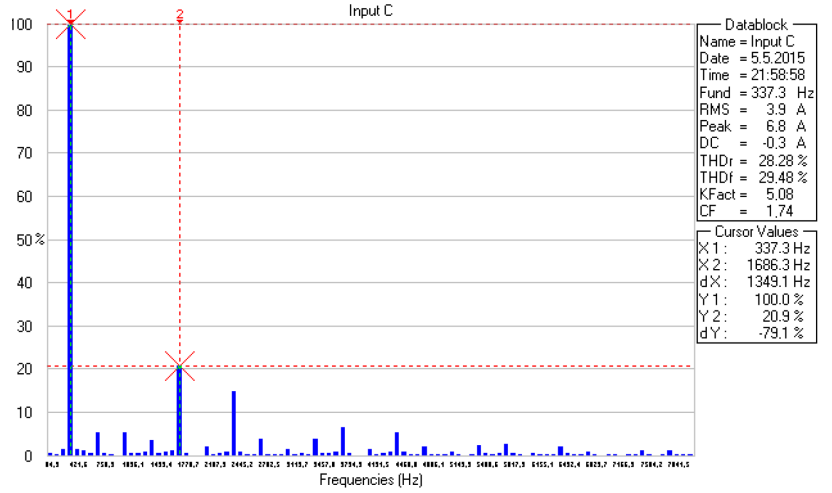

(d)

Figure 11. Continued.

mechanical resonances via adequate increasing of current in a short time. In this work, a current reference method (CRM) was used to protect the power systems of the satellite from the current spikes of the power system.

Thus, the satellite power system is not damaged by the increasing of current without spikes. The current spike has not occurred in the mechanical resonance and speed control has been satisfactorily achieved at that time.

Acknowledgment

The authors would like to thank the Scientific and Technological Research Council of Turkey (TÜBİTAK) for its financial support (Project No: 114E038).

References

[1] Wang L, Yu JY, Chen YT. Dynamic stability improvement of an integrated offshore wind and marine-current farm using a flywheel energy-storage system. IET Renew Power Gen 2011; 5: 387-396.

[2] Gurumurthy SR, Agarwal V, Sharma A. Optimal energy harvesting from a high-speed brushless DC generator-based flywheel energy storage system. IET Electr Power App 2013; 7: 693-700.

[3] Goncalves de Oliveira J, Schettino H, Gama V, Carvalho R. Study on a doubly-fed flywheel machine-based driveline with an AC/DC/AC converter. IET Electric Syst Transp 2012; 2: 51-57.

[4] Briat O, Vinassa JM, Lajnef W, Azzopardi S, Woirgard E. Principle, design and experimental validation of a flywheel-battery hybrid source for heavy-duty electric vehicles. IET Electr Power App 2007; 1: 665-674.

[5] Bharatkar SS, Yanamshetti R, Chatterjee D, Ganguli AK. Simplified design and optimization of slotless synchronous PM machine for micro-satellite electro-mechanical batteries. Adv Electr Comp Eng 2009; 9: 84-88.

[6] Suvire GO, Mercado PE. Combined control of distribution static synchronous compensator/flywheel energy storage system for wind energy applications. IET Gener Transm Dis 2012; 6: 483-492.

[7] Vazquez S, Lukic SM, Galvan E, Franquelo LG. Energy storage system for transport and grid applications. IEEE T Ind Electron 2010; 57: 3881-3895.

[8] Bajec P, Pevec B, Voncina D, Miljavec D, Nastran J. Extending the low-speed operation range of PM generator in automotive applications using novel ac-dc converter control. IEEE T Ind Electron 2005; 52: 436-443.

[9] Takahashi I, Okita Y, Andoh I. Development of long life three-phase UPS using flywheel energy storage unit. In: IEEE 1996 Power Electronics, Drives and Energy Systems for Industrial Growth International Conference; 8–11 January 1996; New Delhi, India; IEEE. pp. 559-564.

[10] Talebi S, Bakhtian BN, Toliyat H. A novel algorithm for designing the PID controllers of high-speed flywheels for traction applications. In: IEEE 2007 Vehicle Power and Propulsion Conference; 9–12 September 2007; Arlington, TX, USA; IEEE. pp. 574-579.

[11] Kenny BH, Kascak PE, Jansen R, Dever T, Santiago W. Control of a high speed flywheel system for energy storage in space applications. IEEE T Ind Appl 2005; 41: 1029-1038.

[12] Aydın K, Aydemir MT. A novel current reference drive method for the control of electric motors used in attitude control systems. J Fac Eng Arch Gazi Univ 2011; 26: 125-138.

[13] Cui C, Liu G, Wang K, Song X. Sensorless drive for high-speed brushless dc motor based on the virtual neutral voltage. IEEE T Power Electr 2015; 30: 3275-3285.

[14] Baszynski M, Pirog S. A novel speed measurement method for a high-speed BLDC motor based on the signals from the rotor position sensor. IEEE T Ind Inform 2014; 10: 84-91.

[15] Aydogmus O. Design of a solar motor drive system fed by a direct-connected photovoltaic array. Adv Electr Comp Eng 2012; 12: 53-58.

[16] Aydın K, Aydemir MT. A control algorithm for a simple flywheel energy storage system to be used in space applications. Turk J Elec Eng & Comp Sci 2013; 21: 1328-1339.

[17] Wai RJ, Lee J.D, Chuang KL. Real-time PID control strategy for maglev transportation system via particle swarm optimization. IEEE T Ind Electron 2011; 58: 629-646.

[18] Abhishek, Ansari MdF. An improved genetic algorithm with variable probability and immune genetic algorithm. International Journal of Advanced Research in Computer Science and Software Engineering 2013; 3: 870-873.

[19] Bist V, Singh B. An adjustable-speed PFC bridgeless buck-boost converter-fed BLDC motor drive. IEEE T Ind Electron 2014; 61: 2665-2677.

[20] Abrahamsson J, Gonçalves de Oliveira J, Santiago J, Lundin J, Bernhoff H. On the efficiency of a two-power-level flywheel-based all-electric driveline. Energies 2012; 5: 2794-2817.

[21] Kenny BH, Santiago W. Filtering and control of high speed motor current in a flywheel energy storage system 2004; Cleveland OH, USA; NASA/TM 2004; 213343.

[22] Awadallah MA, Bayoumi HE, Soliman HM. Adaptive deadbeat controllers DC drives using PSO and ANFIS techniques. J Electr Eng 2009; 60: 3-11.

[23] Fang J, Li W, Li H. Self-compensation of commutation angle based on dc-link current for high-speed brushless dc motors with low inductance. IEEE T Power Electr 2014; 29: 428-439.

[24] Ali MO, Koh SP, Chong KH. Design a PID controller of BLDC motor by using hybrid genetic-immune. Modern Applied Science 2011; 5: 75-85.

[25] Ziegler JG, Nichols N. Optimum settings for automatic controllers. Transactions of the ASME 1942; 65: 759-765.

[26] Vaz AIF, Vicente LN. A particle swarm pattern search method for bound constrained global optimization. J Glob Optim 2007; 39: 197-219.

Appendix

Motor Parameters:

V = 36 V; n = 62,200 rpm; T_m = 35.1 mNm; R_a = 0.122 Ω; L_a = 0.014 mH; K_t = 5.36 mNm/A; K_e = 1780 rpm/V; J = 5.45 g cm^2; B = 0 Nms/rad.

FESS Parameters;

J = 0.0018844 kg m^2; k_f = 1; $\rho_a d_m$ = 18 mm; v = 18 mm^2/s; f_0 = 1.1; f_1 = 0.00037; m = 0.67 kg; g = 9.8 m/s^2; $m_r \times e$ = 665 g mm; r_o = 0.075 m; d = 0.05 m; $L_f = 100 \times 10^{-6}$ H; R_f = 0.022 Ω; $C_f = 1 \times 10^{-6}$ F; K_c = 3.6 V/V; $T_c = 5.36 \times 10^{-5}$ s; K_a = 1 V/A; $T_a = 5.36 \times 10^{-6}$ s, R_1 = 1.8 Ω.